AIAA 98-0288

Experimentation Using the Mir Station as a Space Laboratory

G. F. Karabadzhak, Yu. Plastinin, and B. Khmelinin
Central Institute for Machine Building (TsNIIMASH)
Korolev, Moscow Region, Russia

V. Teslenko and N. Shvets
Energia Space Corporation
Korolev, Moscow Region, Russia

and

J. A. Drakes, D. G. Swann, and W. K. McGregor
Sverdrup Technology, Inc., AEDC Group
Arnold Engineering Development Center
Arnold Air Force Base, Tennessee, USA

36th Aerospace Sciences Meeting& Exhibit
January 12 - 15, 1998 / Reno, NV

Experimentation Using the Mir Station as a Space Laboratory*

*G. F. Karabadzhak,** Yu. Plastinin,** and B. Khmelinin*
Central Institute for Machine Building (TsNIIMASH)
Korolev, Moscow Region, Russia

V. Teslenko and N. Shvets
Energia Space Corporation
Korolev, Moscow Region, Russia

J. A. Drakes,† D. G. Swann, and W. K. McGregor‡
Sverdrup Technology, Inc., AEDC Group
Arnold Engineering Development Center
Arnold Air Force Base, TN 37389-9013 USA

Abstract

Collaboration is now underway to perform space-based experiments on the interactions of rocket plume exhausts and the ambient environment at an altitude of roughly 350 km. The key element in this experiment is the use of the Mir space station as a platform for optical instrumentation. A description is given of the modeling and instrumentation involved in the execution of this experiment, as well as a description of the experiment strategy and some experimental data already obtained. In particular, a hypothesized model of the OH(A-X) ultraviolet radiation is presented and evaluated.

1.0 Introduction

The observation of the emission from electronically excited atoms and molecules in the Earth's uppermost atmosphere has been performed for centuries. An example of this is the aurora. Other more recently discovered examples include the emission from rocket exhaust plumes traveling in the upper atmosphere. It is difficult to recreate the interactions between a rocket exhaust plume and the upper atmosphere environment in a controlled laboratory setting because of the extremely low density of the atmosphere and the large mole fraction of atomic oxygen. In addition, spacecraft are orbiting the Earth at speeds of 5 to 10 km/sec, compared to the essentially static atmosphere. Hence, by virtue of the movement of the spacecraft, there is a high-velocity, low-density atmospheric wind blowing into the rocket exhaust plumes. In addition to the continuing work on mimicking the atmospheric flux in ground test facilities, an additional option is to actually perform the experiments in the space environment. This allows for an *in-situ* evaluation of the chemical kinetics leading to the radiation that is routinely observed during space flights.

The Russian Mir station provides an excellent site for conducting space experiments due to its flexibility and frequent traffic with ground stations. As an example, the Mir will be used as an optical bench in an upcoming experiment, termed MirEx, to observe the generation of the $OH(A^2\Sigma^+ - X^2\Pi)$, $NO(A^2\Sigma^+ - X^2\Pi)$, and $CO(a^3\Pi - X^1\Sigma^+)$ radiation in rocket exhaust plumes and from the interaction of rocket exhaust plumes with the atmosphere. The goal is to determine the chemical excitation pathway that leads to the production of the electronically-excited states. A second objective of this experiment is to evaluate the physical process of vibrational and rotational relaxation of triatomic molecules such as CO_2 as they are rapidly expanded from a high- to low-temperature and density environment. In order to accomplish this experiment, a dedicated maneuver of a Progress supply ship is planned for May 1998. The Progress spacecraft will ignite either the small attitude control thrusters or the larger main engine at precise moments during the undocking trajectory when various portions of the exhaust plume are within the fields of view of the selected onboard optical instrumentation.

Although considerable coordination must be performed during the execution of an experiment such as that mentioned above, it has been found that the Mir station is surprisingly adaptable to such scientific use. The Mir is already populated with numerous spectrometers and radiometric imagers,

* The research reported herein was performed by the Arnold Engineering Development Center (AEDC), Air Force Materiel Command. Work and analysis for this research were performed by personnel of Sverdrup Technology, Inc., AEDC Group, technical services contractor for AEDC. Further reproduction is authorized to satisfy needs of the U. S. Government.

** Member, AIAA.

† Senior Member, AIAA.

‡ Associate Fellow, AIAA.

negating the logistical issue of obtaining flight-rated instrumentation. Furthermore, the frequent travel of the Progress, Soyuz, and U.S. Shuttle to and from the Mir station offers the real possibility of delivering unique special-purpose instrumentation to the station.

As with any experiment, prior planning is key to a successful outcome. This includes the ballistic trajectories for the spacecraft, logistic scheduling for the experiments and cosmonauts or astronauts, and a clear hypothesis to examine in the experiment. For the case of the MirEx experiment, the hypotheses have been, and are continuing to be, modeled to reliably estimate the instrumentation settings. Some processes which may dominate in NO and CO excitation and decay have been studied previously.[1] This paper describes the development of the radiative hypothesis for the OH(A) radiation, the modeling of the expected plume-atmosphere interaction, the assessment of previous data, strategy for experiment execution, and the planned instrumentation. In addition, other types of experiments utilizing the Mir station will be briefly discussed.

2.0 Modeling

2.1 PME Near-Field Radiation

It is important to understand the size and intensity of the expected exhaust plume radiation prior to attempts to measure the radiation. This will be also useful for verification of the models applied. Several methodologies have been used to model potential Mir-based plume experiments. The Progress main engine (PME) exhaust was considered as a primary candidate for observation. The single-nozzle PME utilizes UDMH as the fuel and N_2O_4 as the oxidizer, at an equivalence ratio of 1.85. The area ratio of the PME is 48, with a nozzle exit diameter of 0.3 m. The Progress altitude at the experiment is expected to be between 350 and 400 km. A description of the PME is given in Table 1.

In the near field (order of ten meters from the PME nozzle), the radiation is due to the processes in the plume itself. Further downstream from the nozzle exit, the radiation results mostly from the interaction of the combustion products with the ambient atmosphere. This is because collisions among the combustion products themselves are negligible as the plume expands and the molecules excited in the near field have already decayed. The radiation intensities have been evaluated for the PME plume near field and far field separately. Among a great variety of possible processes resulting in the generation of radiation in the far field, only those are discussed here which produce $OH(A^2\Sigma^+)$ molecules, because some experimental data on the far-field OH radiation have already been obtained.

Table 1. General Characteristics of the Progress Main Engine

Fuel	UDMH
Oxidizer	N_2O_4
Equivalence Ratio	1.85
Chamber Pressure, N/m^2	9.00×10^5
Chamber Temperature, K	2930
Thrust, N	3090
Nozzle Throat Radius, m	0.02445
Nozzle Area Ratio	48

The PME near-field UV and IR radiation intensities in the molecular bands of NO, CO, CO_2 and OH have been evaluated over the maps of gasdynamic parameters by an overlay method using the approximation of an optically thin plume. The Numerical Analysis of Real Jets (NARJ) computer code was employed to generate the gasdynamic parameter maps.[2] NARJ is a fully reacting, axisymmetric, continuum flow solver designed for rocket nozzle and plume computations. Excitation of the plume gas molecular electronic states by solar radiation, geocorona Lyman-alpha, and electronic impact has been considered. Chemical reactions resulting in the plume species excitation have not been considered because modeling of these processes is not finished yet. The PME plume spectral brightness, averaged within 5 meters downstream from the nozzle, has been evaluated for the daytime condition. Table 2 gives the brightness value. The estimated values presented in Table 2 were used as a reference for the experiment planning and are not considered as final results of accurate modeling.

2.2 OH(A) Excitation Mechanisms

There are a number of possible routes to the formation of $OH(A^2\Sigma^+)$ in the rocket exhaust

Table 2. Estimates of the PME Exhaust Plume Brightness in Various Spectral Regions

Molecule	CO	NO	OH	CO_2	CO	NO
Wavelength, mm	0.14-0.17	0.2-0.23	0.3-0.33	4.2-4.4	4.5-4.8	5.1-5.6
Brightness, W/sr-μm-cm^2	10^{-6}	2×10^{-7}	5×10^{-6}	10^{-2}	10^{-3}	10^{-4}

plumes at orbital altitudes, especially in the case of the retrofiring. The most significant constraint on the reaction mechanism is that the very low density will favor two-body reactions over three-body reactions. Hence, the modeling applied to bow shock re-entry vehicles may not be applicable for the present plume problem.[3] However, one similar feature, at least for retrofirings, to the bow shock problem is the high relative velocities between plume exhaust gas molecules and the ambient atmosphere. Given an orbital velocity of 8 km/sec and a typical plume exhaust velocity of 3 km/sec, it is possible to obtain relative velocities in the range of 5 to 11 km/sec. The high level of kinetic energy opens up many possible reaction pathways for $OH(A^2\Sigma^+)$ formation, depending on the details of the conversion of the kinetic energy into internal excitation.

One possibility for creating $OH(A^2\Sigma^+)$ is the two-step reaction of the atmospheric oxygen atoms with plume species such as N_2, given as,

$$O(^3P) + (N_2, O) \rightarrow O(^1D) + (N_2, O) \qquad (1)$$

$$O(^1D) + H_2 \rightarrow OH(A^2\Sigma^+) + H \qquad (2)$$

The formation of the first excited state of atomic oxygen, $O(^1D)$, in a retrofiring plume exhaust has been previously investigated by Murad, et al.[4] The $O(^1D)$ emission was observed by ground telescopes at the US Air Force Maui Observatory (AMOS) during Shuttle vernier engine firings. The engine firings were both wake and ram, and testified to the presence of $O(^1D)$ in the plume due to the interaction with atmospheric oxygen atoms. In the case of $O(^3P)$ and N_2 with a relative velocity of 10 km/sec, the energy excess of Eq. (1) is roughly 3.3 eV, which is an important factor in determining whether the second step proceeds. The second step of the reaction has been investigated in the laboratory by Lebehot, et al.[5] and presents an energy activation barrier of ~2.8 eV, with a net endothermicity of 2.1 eV. Thus, depending upon the final translational energy partitioning of Eq. (1), reaction Eq. (2) may or may not be possible.

A more attractive alternative to the $O(^1D)$ route is the direct formation of $OH(A^2\Sigma^+)$ from the reaction

$$O(^3P) + H_2O \rightarrow OH(A^2\Sigma+) + OH \qquad (3)$$

An extensive discussion of this reaction has been provided by Kofsky, et al.[6] Based upon the endothermicity of the reaction, this process has a threshold relative velocity of 10.4 km/sec. Because the threshold velocity of the reaction is at the higher range of the expected relative velocities, this process can be expected to be relevant primarily for retrofirings. The orbital velocity at the Mir orbit is 7.35 km/sec, allowing only molecules flying in the plume inside the cone with the top half-angle of 22 deg to the spacecraft velocity vector to overcome the reaction threshold. In addition, only those oxygen atoms may produce OH(A) molecules which have not been previously scattered and still possess a velocity anti-parallel to the spacecraft velocity vector in the spacecraft reference center. For simplicity, the $OH(A \rightarrow X)$ is evaluated below for the case of an axisymmetric nozzle with its axis anti-parallel to the spacecraft velocity vector.

2.3 Rarefied Flow Modeling

The NARJ exit plane result was incorporated into a computer code known as SOCRATES[7] (Spacecraft/Orbiter Contamination Representation Accounting for Transiently Emitted Species). The SOCRATES model utilizes the direct simulation Monte Carlo (DSMC) method to simulate the three-dimensional, rarefied gaseous flow-field properties far from the spacecraft. The PME simulation was run with the nozzle exhaust conditions stated in Table 3.

The default atmospheric model of SOCRATES (MSIS '90) was used to define the ambient species

Table 3. PME Exit Plane Predictions, as Determined by NARJ

Altitude, km	350
Vehicle Velocity, km/sec	8
Exit Temperature, K	732
Exit Pressure, N/m^2	1.09×10^3
Exit Density, cm^{-3}	1.08×10^{17}
Exit Velocity, m/sec	2,993
Composition, mole fraction:	
H_2O	0.2884
N_2	0.2668
CO	0.1891
H_2	0.1905
CO_2	0.0531
OH	1.07E-5
H	0.0110
O	9.20E-6

mole fractions and temperatures. For an altitude of 350 km, the atmospheric temperature is 1150 K and the number density is 4.68×10^8 cm^{-3}. The composition is dominated by atomic oxygen, which has a mole fraction of 0.843 at 350 km.

Ideally, to properly characterize the entire flow field of the PME, SOCRATES should be run with cell dimensions that are small enough to provide adequate resolution of the flow-field properties over all space. For the exit plane region of the engine, where the flow-field properties change rapidly, this requires cell dimensions of not more than 1 meter. However, the total region of space occupied by the plume can be on the order of tens of kilometers. Therefore, because of both computer resource and time limitations, the full extent of the PME flow field was simulated using several scaled runs. In all cases the code was run until steady state had been fully reached.

In particular, two SOCRATES computations were performed with cell dimensions of 10 and 100 m . This gave, for the 10-m case, a total computational space of 160 × 160 meters in the cross-sectional plane and 300 meters (250 downstream of the exit plane and 50 meters upstream) along the axial plane. For the 100-m case, the region of space covered was 1,600 × 1,600 × 3,000 meters (2500 m downstream of the nozzle exit plane and 500 m upstream of the nozzle exit plane). These large cell dimensions, however, do not adequately provide flow field properties in the near field of the thruster. Therefore, to characterize the near field (exit plane), a third computation was performed with a cell dimension chosen to be 1 meter. This gave a total computational space of 16 x 16 meters in the cross-sectional plane and 30 meters in the axial plane (25 m downstream of the exit plane of the nozzle and 5 m upstream of the exit plane).

The SOCRATES results for the plume species densities are shown in Figs. 1 and 2. Figure 1 illustrates the predicted total density distribution. For clarity, a cut through the three-dimensional solution domain has been taken along the y = 0 plane (with the orbital velocity vector defining the +z axis), and

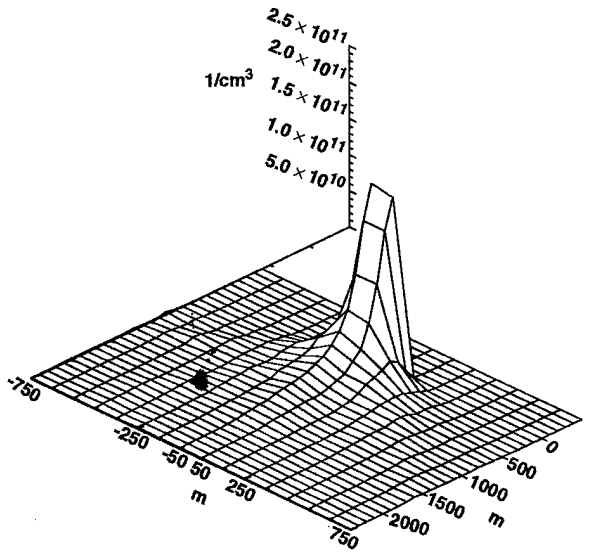

a. Surface map of centerline plane

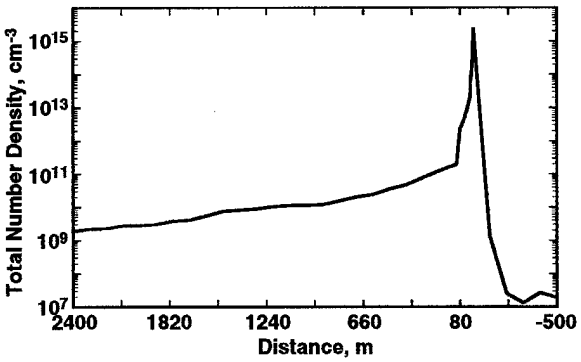

b. Axial Profile

Fig. 1. Calculated total number density of retrofiring Progress plume at 350 km altitude.

is given as a surface map in Fig. 1a. To better illustrate the far-field behavior of the density, the grid spacing in this figure is coarse, as the first grid point after the nozzle exit plane is 50 m downstream. Clearly the rapid expansion of the plume gas into the very low-pressure environment is evident, along with the interesting fan structure of the plume. In Fig. 1b, a profile has been taken of the plume density along the +z axis. In contrast to the surface map shown in Fig. 1a, the profile includes the high spatial resolution solution near the nozzle exit and illustrates the very steep decline of the density, ranging over 5 orders of magnitude in the first 500 meters The behavior of the other major plume species, e.g. H_2O, N_2, H_2, CO and O_2, follow the same trend as the total number density, with the only significant difference being the various scales. This is not unexpected, since the major species chemistry is frozen in the computation.

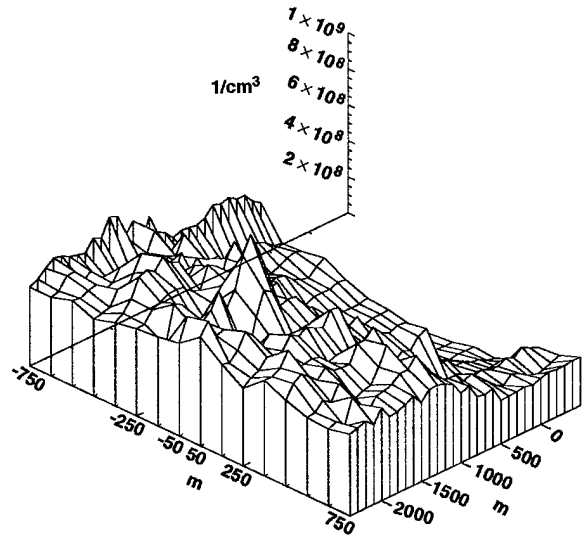

Fig. 2. Calculated atomic oxygen density of retrofiring Progress plume at 350 km altitude.

In marked contrast to the major plume species densities are the atomic O and N densities. Figure 2 shows a surface map of the $O(^3P)$ atom density, analogous to the map of Fig. 1a. For the O atoms, the density is small at the nozzle exit and increases to the ambient atmospheric value as the axial distance is increased. The trend of the O atom density is reversed from the plume species, and illustrates the penetration distance of the atmosphere into the retrofiring plume as roughly to within 500 m downstream of the nozzle exit. The important point to note is that the atmospheric O atoms do not pass through the plume without being scattered by the plume gases. This leaves the region closest to the nozzle comparatively starved for atmospheric O atoms. In the 1-m spatial-resolution calculations, it can be discerned that the O atom density is elevated near the nozzle exit plane due to the O atoms from the plume itself.

Assuming the elastic collision with the plume molecules is the main contributor to the attenuation of the directed flux of the oxygen, the number density, $N_O(x)$,of the reacting oxygen atoms at point x on the plume axis may be expressed as :

$$N_O(x)=N_o \exp(-\int\sigma_{el} N(x')\,dx'), \qquad (4)$$

where N(x) is the total plume number density at point x, N_o is the concentration of the oxygen atoms far away from the spacecraft, and σ_{el} is the elastic collision cross section.

Assuming further that OH(A) molecules produced in the reaction Eq. (3) experience only radiative relaxation, the total amount of radiation in the OH (A→X) band per unit volume in the point x may be calculated:

$$\begin{aligned} B_{ff} &\cong N_{H_2O}(x)\cdot N_O(x)\cdot \sigma_r(v_r)\cdot v_r\cdot h\nu \\ &= N_{H_2O}(x)\cdot N_o \exp(-\int\sigma_{el}N(x')dx') \\ &\quad \cdot \sigma_r(v_r)\cdot v_r\cdot h\nu \end{aligned} \qquad (5)$$

where v_r is the relative velocity between the O atom and the H_2O, and $\sigma_r(v_r)$ is the excitation (reactive) cross section. The dependence of excitation cross section upon the relative velocity for Eq. (3) has been derived in Ref. 6 above,

$$\sigma_r(v_r) = 5.43\cdot 10^{-16}\sqrt{\frac{\left(v_r^2 - v_{th}^2\right)}{v_{th}^2}} \qquad (6)$$

where $\sigma_r(v_r)$ is the reactive cross section in cm^2, and v_{th} is the threshold velocity of 10.4 km/sec. The elastic collision cross section can be estimated, based upon Ref. 6, as 3×10^{-15} cm^{-2}.

Based upon the arguments presented above, the radiation power of the plume per unit volume

may be estimated by Eq. (5). The evaluation made for the PME with the number densities computed from SOCRATES gave a value for B_{ff} = 0.9 W/sr. Furthermore, differentiation of Eq. (5) with respect to the plume axis coordinate, x, gives the coordinate where the specific radiation power is maximal. For the PME computations above, this value is $x_m \approx 630$ meters from the nozzle, indicating that the characteristic cross dimension of the glowing plume region in this case is approximately ~300 meters. However, even a small angle between the velocity vector and the plume axis will result in a decrease of x_m and the characteristic plume dimension in this waveband.

3.0 Instruments and Experimental Scheme

Two spectrometers and an ultraviolet imager have been chosen among the onboard instruments to perform the rocket motor radiation measurements. The NO, CO, and OH emissions related to the electronic transitions will be measured by the VUV-UV spectroradiometer BRIZ. The UV imager equipped with a 310 to 330-nm narrow-band filter will provide the OH(A) radiation spatial distribution. The IR spectrometer ISTOK will measure the CO and NO vibrational band radiation.

3.1. BRIZ Spectrometer

The BRIZ is a four-channel scanning polychromator developed and manufactured in the Optical State Institute in St. Petersburg. It is equipped with four exit slits and four photomultipliers operating in the photon counting mode. It is mounted on top of the SPEKTR-module and connected with cables to the inside data acquisition and control unit. The instrument line of sight is lying in the XY plane of the Mir core module along a line that is 10 deg off the -Y direction to the -X direction. The instrument line-of-sight direction is fixed. The BRIZ instrument works automatically and needs no crew supervision. It uses common Mir data storage and telemetry systems to downlink the data collected. The total time of BRIZ operation is about 15 min per experiment. This time is restricted by the capabilities of the Mir telemetry system. General characteristics of the spectrometer are given in Table 4.

Table 4. BRIZ Spectrometer General Characteristics

Wavelength Region, nm	135-369
Field of View, angular minutes	7×40
Spectral Resolution, nm	2.4 ± 0.3
Scanning Rate, seconds per spectrum	2.0 ± 0.2
Noise Equivalent Radiation declared by Manufacturer, W/sr-μm-cm^2	
$\lambda = 150$ nm	10^{-9}
$\lambda = 250$ nm	10^{-8}
$\lambda = 310$ nm	2×10^{-8}
Dynamic Range	2×10^4

The spectrometer measures spectra simultaneously in four spectral intervals: 135-195 nm, 193-253 nm, 251-311 nm, and 309-369 nm. Accuracy of the interval limits setting is 2 nm. In principle, no overlapping of the intervals is allowed. Accuracy of the wavelength setting is better than 1 nm. Accuracy of the noise equivalent radiation data as declared by the instrument manufacturer is better than 30 percent in the region of λ =200-369 nm and better than 40 percent in the region of $\lambda < 200$ nm. The spectrometer has a built-in calibration source that automatically provides a reference spectrum after every 300 sec of operation.

3.2. The UV Imager

The UV imager was developed and manufactured at TSNIIMASH in cooperation with the Optical Department of Lebedev's Physical Institute. It combines a quartz telescope followed by an image intensifier and relay lens to interface with a radiation detector. To effectively block the visible radiation a solar blind Cs_2Te photocathode is used in the image intensifier. The UV imager is also equipped with a broad-band color glass UV filter and three different narrow-band (8-nm FWHM) interference filters. Some general characteristics of the UV imager are presented in Table 5.

Table 5. UV-Imager General Characteristics

Operating Wavelength Region, nm	200 - 360
Wide Band Color UV Filter, nm	240 - 360
Interference Filter's Centers, nm	260, 284, 317
Telescope Effective Diameter, mm	55
Telescope Focal Length, mm	78
Field of View, deg	12
Angular Resolution, angular minutes	3.0
Image Intensifier Maximum Gain	$\sim 3 \times 10^4$

The imager is located inside the Mir station and, can therefore work effectively only when looking through a quartz window. Common photo and video cameras are basically used as the detecting element. Modular design of the UV imager provides an opportunity to easily replace the detector in accordance with experiment requirements. The crew operator can observe the imaging scene through the detector viewfinder. There was also a provision to set the image intensifier amplification gain at the level appropriate to the radiance of the object being observed. Crewmembers are trained to handle the imager before flight and will be provided with a specific experiment plan from the Mission Control Center just before the experiment.

The use of video tapes and photo films for data recording, storage and delivery simplifies the data acquisition system, but it brings forth severe requirements to the imager calibration procedure when absolute radiation values are to be measured. The used films are returned to Earth by the next Progress cargo spacecraft flight. The most interesting and urgent data are recorded on videotape and may be promptly transmitted to the Mission Control Center terminals in the course of a regular TV session.

The Mir station has two quartz windows and special window adapter for the UV imager mounting. The line of sight of the UV imager during operation can be either firmly fixed along a specified direction with respect to the window axis or controlled by the crew operator.

The absolute sensitivity of the imager is not presented in the Table 5 because it depends on the window transparency and on the particular detector and recording tape characteristics. On those occasions when absolute values of radiation have to be reduced from the images obtained, the imager is accurately calibrated against known radiation from various stars, using the identical experimental arrangement. Analysis of the data obtained from the UV imager for four years of its operation indicates that the spectral response of the instrument is largely defined by the image intensifier spectral sensitivity and the filter transparency curve in the region $\lambda > 270$ nm. Therefore, absolute response of the instrument at the center of narrowband filter $S(\lambda_0)$ may be derived from:

$$P_s = S(\lambda_0) \int E(\lambda) \cdot T(\lambda) \cdot s(\lambda) \cdot d\lambda, \qquad (7)$$

where $E(\lambda)$ - star radiation flux, $T(\lambda)$ - filter transparency, $s(\lambda)$ - image intensifier relative spectral sensitivity.

3.3. ISTOK Spectrometer

The ISTOK instrument was developed and manufactured in the Optical Department of Lebedev's Physical Institute of Russian Academy of Sciences in Moscow. It combines several units: optical, electronic, calibration source unit, data acquisition and control unit and some others. The optical unit is located outside the PRIRODA module on the rotating platform. Its line of sight may be positioned before measurement along any preset direction inside the field of regard, which covers all the space confined by the +X, +Y, +Z axes of the Mir core module. The optical unit of the instrument consists of two identical channels. The first channel provides the spectrum in the region of λ = 4-8 μm, and the other in the region λ = 8-16 μm. The incoming radiation dispersed on the grating is detected by a 32-pixel linear array of pyroelectric detectors in the spectrometer. The spectrometer has a built-in mechanical chopper for the radiation flux frequency modulation. The spectrometer works automatically and doesn't need crew supervision. Measurements are controlled by an onboard control unit which in turn works in accordance with the instructions uplinked from the Mir Mission Control Center during routine telemetry sessions. All housekeeping and scientific data are written in the spectrometer digital memory unit onboard the Mir station and stored there until next telemetry session. The spectrometer can work continuously for more than 15 min. The operating time is basically restricted by the capacity of the data storage system.

Some general characteristics of the ISTOK spectrometer are given in Table 6.

3.4 Strategy of the Experiment

Comparison of the expected radiation intensity with the instruments' sensitivities and fields of view shows that near-field emissions spectra of the PME exhaust could be reliably measured from distances of less than several kilometers. Measurements of the far-field PME radiation spectra and

ACS thruster's emissions may require an even smaller distances. Hence, the firing of these motors during the spacecraft docking and undocking procedures represents an ideal opportunity for observation. Several attempts were made last year to measure the spectra during the Shuttle and Progress undocking; however, no reliable data have been obtained from these attempts. This was primarily because in those instances, the spacecraft docking and undocking were very intensive procedures, requiring unique station orientation and consuming much of the station resources and crew attention as well. While continuing with the attempts to measure the motor exhaust radiation spectra during undocking, a dedicated Progress plume observation experiment was planned for last fall. Figure 3 helps to understand the strategy of the experiment. The black squares in this figure represent points of the Progress trajectory after undocking. Distances on the axes are given in km in the frame system referenced to the Mir station. Also, times after undocking are shown at the picture when the firings will take place.

Table 6. Some General Characteristics of the ISTOK Spectrometer

Operating Wavelength Region, μm	4-16
Spectral Resolution, μm:	
in the region 4-8 μm	0.125
in the region 8-16 μm	0.250
Sensitivity Level for 1-Hz bandpass, $W/cm^2 \cdot sr \cdot \mu m$:	
in the region 4-8 μm	10^{-5}
in the region 8-16 μm	5×10^{-6}
Dynamic Range	$>10^2$
Minimum Time per Spectrum Acquisition, sec	1
Field of View, angular minutes	6.5×26

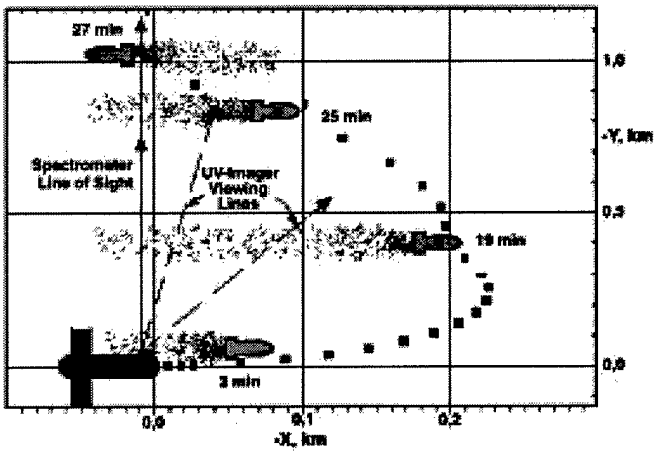

Fig. 3. Planned Progress trajectory and plume positions during observation event, Earth is below and both Mir and Progress are moving to the right.

The experiment was to be performed right after the Progress undocking. During undocking, the station supports an orbital orientation (maintains a fixed position referenced to the Earth system frame). In this orientation the X axis of the MIR Core module lies in the orbital plane, and the Y axis either lies in the orbital plane or directed perpendicular to it. The spacecraft detaches the station mechanically and goes forward and up from the station in the direction of the velocity vector, flying over the station toward its rear side. In the course of this maneuver, the spacecraft was scheduled to perform three dedicated ACS motor firings of about 10-sec duration each. As is seen from Fig. 3, the spectrometers were supposed to measure the exhaust spectra from different parts of the plume while one of the crewmembers manually tracked the spacecraft with the UV imager.

The summer accident seriously impacted all scientific activity onboard the MIR station. The scientific program was suspended and only recently recovered. The dedicated plume observation experiment is now being planned for May. Although no reliable spectra have been obtained due to above-mentioned reasons, some data from the UV-imager appeared to be quite interesting and demonstrated the ability to perform the plume observation experiments onboard the Mir station.

4.0 Results of the Preliminary Experiments

The UV imager filtered in the $\lambda = 280$ to 330-nm wavelength region was used to observe retrofirings of the Progress main engine. The main engine retrofirings are being performed each time the Progress de-orbit before its re-entry. The engine operates for about 4 min during this maneuver, and the distance to the spacecraft ranges from about 12 km to about 60 km, depending on particular requirements of the re-entry conditions. The

spacecraft positions itself before the firing in such a way as to keep the X axis (plume centerline) in the orbital plane and parallel to the velocity vector. Once the engine is fired, the spacecraft keeps inertial orientation, resulting in continuous changing of the plume axis direction with respect to the velocity vector. The Mir station orientation is normally the inertial one during the Progress re-entry. However, the station can build, in principle, a specific orientation that corresponds to the observation requirements and provides proper spacecraft viewing.

The general scheme of the Progress retrofiring observation is as depicted in Fig. 4. A specific peculiarity of the observation is that Progress main axis is always located inside the angle ± 20 deg from the line of sight, such that the PME nozzle throat may be seen from Mir. Table 7 gives the observation conditions and Fig. 5 represents three typical samples of images obtained in the experiments.

The plume images in Fig. 5 are essentially diffused and differ from a star point source image.

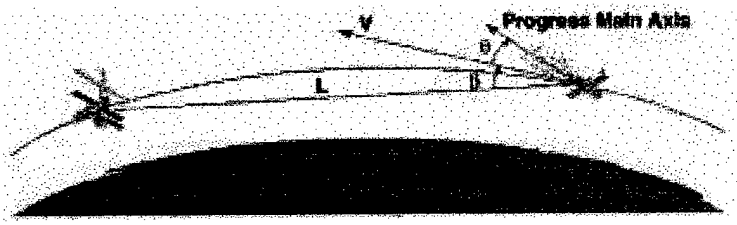

Fig. 4. Schematic of viewing geometry of Mir and Progress after undocking.

Table 7. Progress Main Engine Plume Observation Conditions

Sample #	Distance to the Progress, km	Angle β (see Fig.6), deg	Angle θ, deg
a	15.8	3.6	7.7
b	19.7	- 0.2	11.6
c	22.3	- 2.4	16.0

Based on the stellar images analysis, the UV imager angular resolution was evaluated to be equal about $1.7 \cdot 10^{-3}$ rad full-width at half–maximum (FWHM). Allowing for this resolution, the spatial scale of the radiating volume cross section recovered from the images appeared to be about 70-80 meters. Assuming the radiation in the considered wavelength region is mainly due to the OH($A^2\Sigma^+ \rightarrow X^2\Pi$) transition, its intensity was evaluated based on the imager calibration data. The intensity appeared to be B = 1.2 ± 0.3 W/sr.

Because of the experiment geometry, the total radiation is a combination of radiation from the combustion chamber/intrinsic nozzle, as well as the near-field and far-field plume components. The combustion chamber/intrinsic nozzle radiation yield was evaluated, assuming that combustions product composition and excited states population, correspond to the local thermodynamic equilibrium condition. The radiation transfer equation

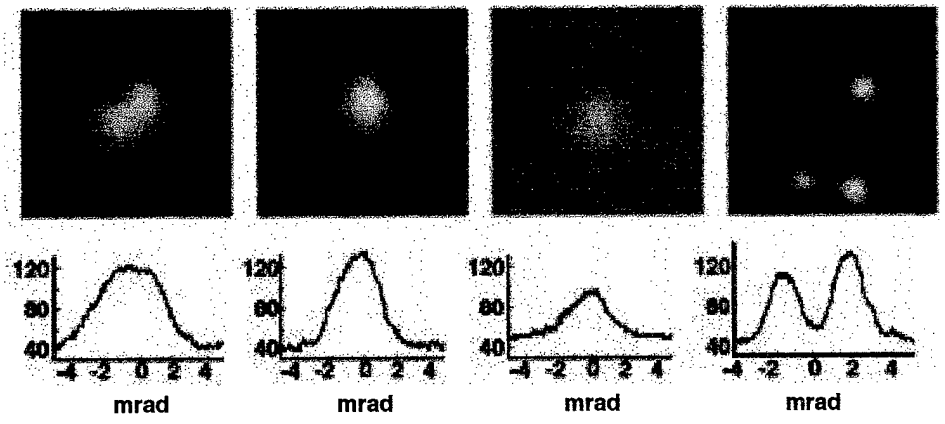

Fig. 5. Progress plume images and Pleiades stellar cluster image clip (the same magnification). Intensity profiles taken approximately at the middle of the images are shown below the image.

was integrated along the nozzle axis, accounting for re-absorption of the radiation by a cold gas. The result of that exercise was an estimated chamber intensity of $B_{ch} \cong 0.12$ W/sr, which is noticeably less than measured intensity. The near-field radiation estimated in Section 2.1 is even less. In addition, the combustion chamber and near field radiating volume characteristic dimension does not correspond to the measured scales.

The observation results may be reasonably explained if the chemical reaction Eq. (3) between the atmospheric oxygen atoms and water molecules in the far field is taken into account. The $OH(A^2\Sigma^+ \rightarrow X^2\Pi)$ far-field radiation intensity value, B_{ff}, from Section 2.2, complemented by the combustion chamber radiation, B_{ch}, agrees reasonably with the experimental results. Moreover, spatial scale of the radiating volume estimated in Section 2.2 corresponds roughly to that obtained in the experiment.

According to the radiation model suggested above, the region of maximal specific radiation power must be detached from the nozzle and a relatively dark gap between the radiating nozzle and far-field region must be evident. Perhaps this might happen if the viewing angle with respect to the spacecraft velocity vector (β in Table 7) was larger. The largest angle in the experiment was $\beta = 3.62$ deg. The dark gap of a several hundred-meter scale would have $0.5\text{-}1.0 \times 10^{-3}$ rad angular dimension, or about two times smaller than the imager angular resolution. However, some trend to a gap formation may be supposed in the image shown in Fig. 5a. Further experiments onboard the Mir station will help to study this phenomenon in quarter detail.

5.0 Other Experiment Opportunities

Among other opportunities of multi-spectral observations onboard the Mir station, the Progress re-entry, Earth limb, and upper atmosphere observation are certainly worth mentioning. The Mir station is currently carrying a set of spectral instruments covering the wavelength region from 0.13 through 16 μm. The imager set available onboard includes a variety of visible/near-IR cameras provided with narrow-band filters, as well as the UV imager. A complete discussion on possible applications of the instruments lies beyond the scope of the present paper, and only a brief example of the UV imager application in observation of spatial distribution of the Progress re-entry signature is given below.

The advantage of the observation in the UV region is that it may be performed on the day side of the orbit, when observation in the visible region is not very effective due to relatively high Earth background. Figure 6 shows samples of Progress re-entry images taken both at night (a) and day (b) conditions.

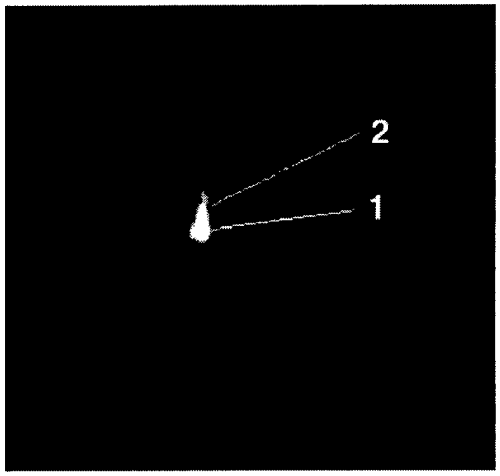

a. Night side, altitude - 60km, distance - 540 km (magnified image)

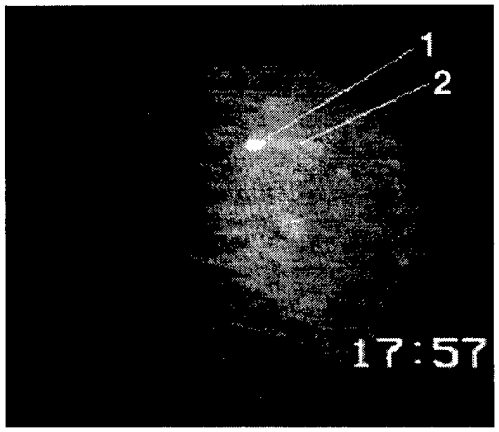

b. Day side, altitude - 66 km, distance 360 km

Fig. 6. UV-image of the Progress spacecraft during its reentry into the Earth atmosphere; (1) spacecraft region, (2) wake region.

6.0 Conclusion

A complex experiment is being planned onboard the Mir station to study high-altitude combustion exhaust emissions and the outflow interaction with rarefied ambient atmosphere. In anticipation of the experiment, the Progress spacecraft main engine flow field has been modeled and expected far-field $OH(A^2\Sigma^+ \rightarrow X^2\Pi)$ radiation intensity has been evaluated basing on this modeling.

Relatively intensive far-field radiation in the region of 280 to 330 nm has already been discovered in the course of preliminary observations of the PME retrofirings. A possible explanation of the phenomena is the formation of excited OH molecules in chemical reaction between atmospheric oxygen atoms and water molecules available in the PME exhaust. The suggested model resulted in the inference that the glowing region must be detached from the spacecraft's body, due to inevitable and complete scattering of the atmospheric oxygen flux on the exhaust plume. This fact opens up a way to accurately recover the excitation cross section from the measured value of integral far-field radiation. The upcoming experiments will hopefully provide new valuable data for current model verification.

7.0 Acknowledgments

The authors would like to thank E. Szhenov, G. Sipatchev, and A. Afanasjev, A. Rodionov and G. Baula from TsNIIMASH for their valuable help in the experiment arrangements and for obtaining data processing. We appreciate the immensely high efficiency of V.Kukushkin and O.Volkov from Energia Space Corporation in the experiment's planning and promotion. Finally, we wish to express our special thanks to Professor N. Anfimov for his continuous interest in this work, and for his useful comments.

References

1. Drakes, J. A., McGregor, W. K., and Nelius, M. A., "Mechanism for NO(A-X) Radiation in a Low-Pressure Combustion Exhaust," AIAA 96-1880, 31st AIAA Thermophysics Conference, New Orleans, 1996.

2. Rodionov, A., "NARJ Software Package (Numerical Analysis of Real Jets), Version 97," TsNIIMASH, 1997.

3. Levin, D. A., Candler, G. V., and Collins, R. J., "An Overlay Method for Calculating Excited State Species Properties in Hypersonic Flows," AIAA 95-2073, 30th AIAA Thermophysics Conference, San Diego, 1995.

4. Murad, E., Knecht, D. J., Viereck, R. A., Pike, C. P., Kofsky, I. L., Trowbridge, C. A., Rall, D. L., Ashley, G., Twist, L., Elgin, J. B., Setayesh, A., Stair, A. T., and Blaha, J. E., "Visible Light Emission Excited by Interaction of Space Shuttle Exhaust with the Atmosphere," *Geophysical Research Letters*, Vol. 17, 1990, pp. 2205.

5. Lebehot, A., Drawin, S., Aguillon, F., Campargue, R., and Chapuisat, X., *J. Chem Phys*, Vol. 92, 1990, pp. 7340.

6. Kofsky, I. L., Barret, J. L., Brownrigg, T. E., McNicholl, P. N., Tran, N. H., and Trowbridge, C. A., "Excitation and Diagnostics of Optical Contamination in the Spacecraft Environment," AFGL-TR-88-0393, 1988.

7. Elgin, J. and Bernstein, L. S. "The Theory Behind the SOCRATES Code," PL-TR-92-2207, 1992.

REPORT DOCUMENTATION PAGE

Form Approved
OMB No. 0704-0188

1. AGENCY USE ONLY *(Leave blank)*	2. REPORT DATE	3. REPORT TYPE AND DATES COVERED
	January 1998	Technical Society Paper

4. TITLE AND SUBTITLE
Experimentation Using the Mir Station as a Space Laboratory
AIAA Paper No. 98-0288

5. FUNDING NUMBERS

6. AUTHOR(S)
G. F. Karabadzhak, Yu. Plastinin, B. Khmelin, V.Teslenko, N. Shvets, J. A. Drakes, D. G. Swann, and W. K. McGregor

7. PERFORMING ORGANIZATION NAME(S) AND ADDRESS(ES)
TsNIIMASH, Korolev, Moscow Region, Russia;
Energia Space Corporation, Korolev, Moscow Region, Russia;
Sverdrup Technology, Inc., AEDC Group, Arnold AFB, TN 37389

8. PERFORMING ORGANIZATION REPORT NUMBER

9. SPONSORING/MONITORING AGENCY NAME(S) AND ADDRESS(ES)
AEDC/DOS
Arnold AFB, TN 37389

10. SPONSORING/MONITORING AGENCY REPORT NUMBER

11. SUPPLEMENTARY NOTES
Presented at 36th Aerospace Sciences Meeting & Exhibit in Reno, NV.

12a. DISTRIBUTION AVAILABILITY STATEMENT
Approved for public release; distribution unlimited.

12b. DISTRIBUTION CODE
A

13. ABSTRACT *(Maximum 200 words)*

Collaboration is now underway to perform space-based experiments on the interactions of rocket plume exhausts and the ambient environment at an altitude of roughly 350 km. The key element in this experiment is the use of the Mir space station as a platform for optical instrumentation. A description is given of the modeling and instrumentation involved in the execution of this experiment, as well as a description of the experiment strategy and some experimental data already obtained. In particular, a hypothesized model of the OH(A-X) ultraviolet radiation is presented and evaluated.

14. SUBJECT TERMS
Mir, UV Radiation, Plumes

15. NUMBER OF PAGES
12

16. PRICE CODE

17. SECURITY CLASSIFICATION OF REPORT	18. SECURITY CLASSIFICATION OF THIS PAGE	19. SECURITY CLASSIFICATION OF ABSTRACT	20. LIMITATION OF ABSTRACT
Unclassified	Unclassified	Unclassified	UL